Available online at www.sciencedirect.com
ScienceDirect
Composites: Part B 39 (2008) 714–721
composites Part B: engineering
www.elsevier.com/locate/compositesb

Investigating thermal residual stress effect on mechanical behaviors of fiber composites with different fiber arrays

Jia-Lin Tsai *, Yang-Kai Chi

Department of Mechanical Engineering, National Chiao Tung University, Hsinchu 300, Taiwan

Received 1 April 2007; accepted 25 May 2007
Available online 22 June 2007

Abstract

This study aims to investigate the thermal residual stress effect on the constitutive behaviors of fiber composites with three different fiber arrays, i.e., square edge packing, square diagonal packing, and hexagonal packing. The repeating unit cell (RUC) containing fiber and matrix phase was employed to describe the mechanical behaviors of fiber composites. For the fiber phase, it was assumed to be linear elastic, whereas the matrix was a nonlinear material. The generalized method of cell (GMC) micromechanical model originally proposed by Paley and Aboudi [Paley M, Aboudi J. Micromechanical analysis of composites by the generalized cells model. Mech Mater 1992; 14(2):127–39] was extended to include the thermal–mechanical behavior, from which the thermal residual stress within the fiber and matrix phases was calculated. Through numerical iteration, the constitutive relations of the composites in the presence of residual stress were established. Results show that for the composites with square edge packing, the mechanical behaviors are affected appreciably by the thermal residual stress. On the other hand, the composites with hexagonal packing and square diagonal packing are relatively less sensitive to the thermal residual stress.

Keywords: A. Fiber array; B. Nonlinear behavior; B. Thermal residual stress; C. Micromechanical analysis

1. Introduction

Fiber composites, because of their superior mechanical performances and light weight properties, have been extensively employed in various applications. In the manufacturing process, the fiber composites were usually cured at high temperatures followed by the cooling stage to room temperature. During the cooling, because of the mismatch in the coefficients of thermal expansion of the fiber and matrix together with the mutual constraint effect, the thermal residual stress was induced in the constituents. The magnitude of the residual stress relies on the properties of the fiber and matrix as well as the associated microstructures of the fiber composites, including the fiber shape and fiber packing arrangements. In addition, the formation of residual stress may have influences on the constitutive behaviors of the fiber composites, especially in the nonlinear range because the nonlinear behavior is highly dependent on the stress states of the composites.

The constitutive behaviors of the composites with different fiber architectures have been characterized by many researchers using either finite element analysis or analytical micromechanical approach [2–6]. Zhu and Sun [2] investigated the nonlinear behaviors of AS4/PEEK composites with three different fiber arrays under off-axis loading using finite element approach. It was found that the nonlinear behaviors of the composites were quite sensitive to the fiber packing arrangement. The similar conclusions were also addressed by Hsu et al. [3], who proposed an analytical micromechanical model for simulating the nonlinearity of AS4/PEEK composites subjected to combined transverse compression and shear loading. Orozco and Pindera [4] conducted a micromechanical analysis using the GMC model on the two-phase composites with randomly

* Corresponding author. Tel.: +886 3 5731608.
E-mail address: jialin@mail.nctu.edu.tw (J.-L. Tsai).

1359-8368/$ - see front matter © 2007 Elsevier Ltd. All rights reserved.
doi:10.1016/j.compositesb.2007.05.005

distributed fibers, indicating that as the number of the refined sub-cells in the unit cell is increased, the behaviors of the composites tend to be that of a transversely isotropic solid. The influences of fiber shape and fiber distribution on the elastic/plastic behavior of metal matrix composites were examined by Pindera and Bednarcyk [5] using the GMC micromechanical model. It was shown that the fiber packing exhibits a substantially greater effect on the responses of the composite materials than does the fiber shape. Pindera et al. [6] investigated the nonlinear behaviors of the boron/aluminum composites subjected to tensile, compressive and off-axis loadings. The thermal residual stress was considered in their analysis in order to explain the differences of initial yielding in tension and compression. The effect of residual stresses on yielding of SiC/Ti plates was also reported by Zhou et al. [7]. Aghdam et al. [8] accounts for residual stresses, off-axis orientation and the interface condition between fiber and matrix on the constitutive behaviors of SiC/Ti metal matrix composites. However, their analysis is limited to single fiber array (square). A comprehensive review regarding the effect of fiber arrangement on the elastic and inelastic responses of fiber composites was provided by Arnold et al. [9]. In light of the aforementioned investigations, it was suggested that the behaviors of the fiber composites were mainly dominated by the fiber packing arrangements. However, few studies concerning the influence of the residual stress arising from curing associated with different fiber arrays on the performances of fiber composites have been reported.

The objective of this study is to investigate the effect of thermal stress on the stress and strain curves of composites with different fiber packing arrangements. An appropriate repeating unit cell (RUC) corresponding to each fiber array was selected for the micromechanical analysis where the fiber was considered to be linear elastic, and the matrix was assumed to follow the nonlinearity of von Mises J_2 materials. By using Aboudi's GMC micromechanical model [1], the incremental form of the constitutive relations of the composites was expressed in terms of the constituent properties as well as the geometry parameters of the RUC, from which the thermal residual stress within the ingredients was calculated. After a numerical iteration, the corresponding stress and strain relations of the composites in the presence of thermal residual stress subjected to off-axis loading were generated. The results were compared to those calculated from the composites without taking into account the thermal stress effect.

2. Micromechanical approach

2.1. Selection of unit cell

In modeling the mechanical responses of fiber composites using a micromechanical approach, a unit cell needs to be properly selected to represent the microstructures of the materials, and thus, the overall composites responses can be predicted directly from the unit cell. In this study, three different fiber arrays, i.e., square edge packing, square diagonal packing, and hexagonal packing, were considered and illustrated, respectively, in Fig. 1. Based on the periodicity and symmetry conditions in the uniformly distributed fibers, the repeating unit cells (RUCs) enclosed with dashed lines in Fig. 1 were chosen and utilized to obtain the mechanical properties of the fiber composites associated with different fiber arrangements [10].

2.2. Characterization of matrix nonlinearity

In order to characterize the behavior of the fiber composites using the micromechanical approach, the constitutive properties of the constitutions, i.e., fiber and matrix, as well as the fiber volume fraction have to be specified initially. In the research, the fiber was assumed to be linear elastic materials, whereas the matrix phase was regarded as a nonlinear material. To model the nonlinear deformation, the matrix was assumed to be von Mises J_2 materials, and through the flow rule, the plastic strain increment of the matrix was expressed as

$$\mathrm{d}\varepsilon_{ij}^{\mathrm{p}} = \mathrm{d}\lambda \frac{\partial J_2}{\partial \sigma_{ij}} \tag{1}$$

where

$$J_2 = \frac{1}{6}\left[(\sigma_{11}-\sigma_{22})^2 + (\sigma_{22}-\sigma_{33})^2 + (\sigma_{33}-\sigma_{11})^2\right] + \sigma_{12}^2 + \sigma_{23}^2 + \sigma_{13}^2 \tag{2}$$

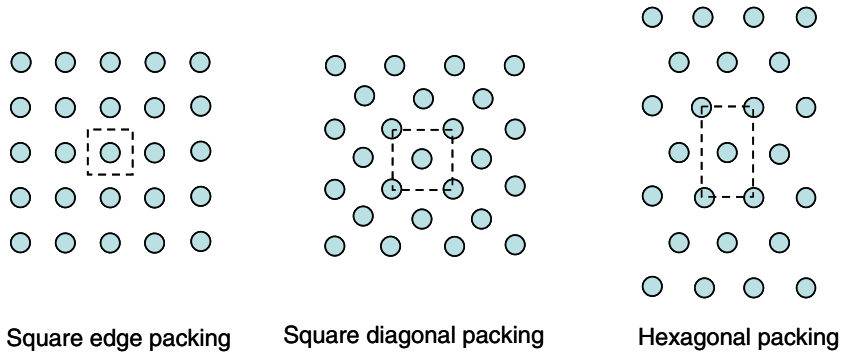

Fig. 1. Three different fiber packing arrangements for fiber composites.

and $d\lambda$ is a proportional factor.

By defining an effective stress $\bar{\sigma}$ as

$$\bar{\sigma} = \sqrt{3J_2} \tag{3}$$

through the equivalence of plastic work, i.e.,

$$dW^p = \sigma_{ij}\, d\varepsilon_{ij}^p = \bar{\sigma}\, d\overline{\varepsilon^p} = 2J_2\, d\lambda \tag{4}$$

the effective plastic strain increment $d\overline{\varepsilon^p}$ was given explicitly as

$$d\overline{\varepsilon^p} = \frac{2}{3}\left\{\frac{1}{2}[(d\varepsilon_{11}^p - d\varepsilon_{22}^p)^2 + (d\varepsilon_{22}^p - d\varepsilon_{33}^p)^2 + (d\varepsilon_{33}^p - d\varepsilon_{11}^p)^2] + \frac{3}{4}(d\gamma_{12}^{p^2} + d\gamma_{23}^{p^2} + d\gamma_{13}^{p^2})\right\}^{1/2} \tag{5}$$

and the proportional factor $d\lambda$ in Eq. (1) was derived as

$$d\lambda = \frac{3}{2}\frac{d\overline{\varepsilon^p}}{\bar{\sigma}} = \frac{3}{2}\frac{d\bar{\sigma}}{H_p\bar{\sigma}} \tag{6}$$

where H_p is the plastic modulus and written as

$$H_p = \frac{d\bar{\sigma}}{d\overline{\varepsilon^p}} \tag{7}$$

In addition, the relationship of effective stress and effective plastic strain is assumed to be described using a power law function as

$$\overline{\varepsilon^p} = A(\bar{\sigma})^n \tag{8}$$

With Eqs. (7) and (8), the plastic modulus $d\lambda$ is yielded as

$$H_p = \frac{1}{nA(\bar{\sigma})^{n-1}} \tag{9}$$

Based on the definition of the effective stress given in Eq. (3), $d\bar{\sigma}$ is deduced explicitly as

$$d\bar{\sigma} = \frac{1}{2\bar{\sigma}}[(2\sigma_{11} - \sigma_{22} - \sigma_{33})d\sigma_{11} + (-\sigma_{11} + 2\sigma_{22} - \sigma_{33})d\sigma_{22} + (-\sigma_{11} - \sigma_{22} + 2\sigma_{33})d\sigma_{33} + 6\sigma_{23}\, d\sigma_{23} + 6\sigma_{13}\, d\sigma_{13} + 6\sigma_{12}\, d\sigma_{12}] \tag{10}$$

By substituting Eq. (10) together with Eq. (6) into Eq. (1), the plastic strain increment is written explicitly in terms of the stress increments as

$$\begin{Bmatrix} d\varepsilon_{11}^p \\ d\varepsilon_{22}^p \\ d\varepsilon_{33}^p \\ d\gamma_{23}^p \\ d\gamma_{13}^p \\ d\gamma_{12}^p \end{Bmatrix} = \frac{9}{4}\frac{1}{H_p\bar{\sigma}^2}\begin{bmatrix} S_1^2 & S_1S_2 & S_1S_3 & S_1S_4 & S_1S_5 & S_1S_6 \\ & S_2^2 & S_2S_3 & S_2S_4 & S_2S_5 & S_2S_6 \\ & & S_3^2 & S_3S_4 & S_3S_5 & S_3S_6 \\ & \text{symmetric} & & S_4^2 & S_4S_5 & S_4S_6 \\ & & & & S_5^2 & S_5S_6 \\ & & & & & S_6^2 \end{bmatrix} \times \begin{Bmatrix} d\sigma_{11} \\ d\sigma_{22} \\ d\sigma_{33} \\ d\sigma_{23} \\ d\sigma_{13} \\ d\sigma_{12} \end{Bmatrix} \tag{11}$$

where

$$S_1 = \frac{1}{3}(2\sigma_{11} - \sigma_{22} - \sigma_{33})$$
$$S_2 = \frac{1}{3}(-\sigma_{11} + 2\sigma_{22} - \sigma_{33})$$
$$S_3 = \frac{1}{3}(-\sigma_{11} - \sigma_{22} + 2\sigma_{33})$$
$$S_4 = 2\sigma_{23}$$
$$S_5 = 2\sigma_{13}$$
$$S_6 = 2\sigma_{12}$$

It is noted that in Eq. (11), the elements in the plastic compliance matrix are not a constant, but they dependent on the stress states, and for a given loading history, a numerical iteration process is usually required to update the compliance matrix. By combining the elastic parts, the incremental form of the constitutive relation of the epoxy material is established as

$$\{d\varepsilon\} = [S^M]\{d\sigma\} \tag{12}$$

where

$$[S^M] = [S^e] + [S^p] \tag{13}$$

In Eq. (13), $[S^e]$ represents the elastic compliance matrix of the epoxy, and $[S^p]$ denotes the plastic compliance matrix given in Eq. (11). By inverting Eq. (12), the stress and strain relation expressed in terms of the stiffness matrix is obtained as

$$\{d\sigma\} = [C^M]\{d\varepsilon\} \tag{14}$$

where

$$[C^M] = [S^M]^{-1} \tag{15}$$

Therefore, the constitutive relation given in Eq. (14) will be utilized afterward in the micromechanical model to denote the matrix materials properties. It should be noted that the incremental plasticity equations implemented into the GMC framework are different from those employed by Pindera and Bednarcyk [5] and Arnold et al. [9].

2.3. Generalized method of cells

With the ingredient properties and the properly selected RUC, the mechanical behavior of fiber composites can be simulated using the generalized method of cells (GMC) micromechanical model proposed originally by Paley and Aboudi [1]. It is noted that in the GMC analysis, the RUC is usually divided into $N_\beta \times N_\gamma$ sub-cells as shown in Fig. 2. Based on the displacement continuity on the interface of the adjacent sub-cells in conjunction with the periodicity condition of the RUC, the relation between overall strain rates and the sub-cell strain rates is expressed as [1]

$$A_G\eta_s = J\bar{\eta} \tag{16}$$

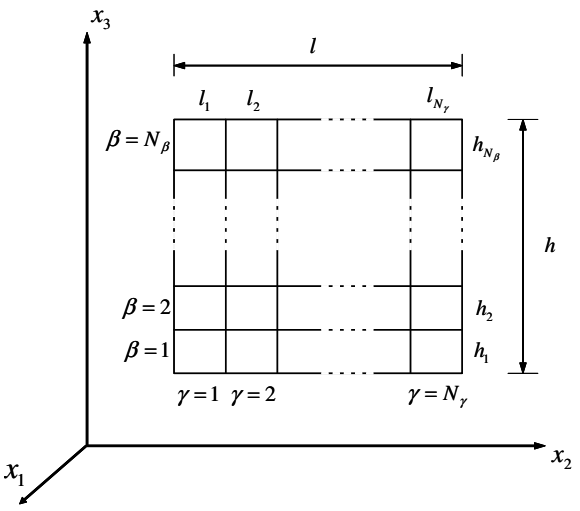

Fig. 2. A typical RUC portioned into $N_\beta \times N_\gamma$ sub-cells in GMC analysis [1].

where $\eta_s = \{\bar{\eta}^{(11)}, \bar{\eta}^{(12)}, \ldots, \bar{\eta}^{(N_\beta N_\gamma)}\}$ represents the collection of the engineering strain increments for all sub-cells, and $\bar{\eta} = \{\bar{\eta}_{11}, \bar{\eta}_{22}, \bar{\eta}_{33}, 2\bar{\eta}_{23}, 2\bar{\eta}_{13}, 2\bar{\eta}_{12}\}$ indicates the overall strain increments of the RUC. In addition, A_G and J contain geometry parameters of the sub-cells and the RUC, the dimension of which are $2(N_\beta + N_\gamma) + N_\beta N_\gamma + 1$ by $6N_\beta N_\gamma$ and $2(N_\beta + N_\gamma) + N_\beta N_\gamma + 1$ by 6, respectively.

In addition, from the traction continuity of the sub-cells, the relation of sub-cell strain increment is established as

$$A_M^{VP} \eta_s = 0 \tag{17}$$

where A_M^{VP} involves material properties of the sub-cells. Combining Eqs. (16) and (17) leads to the following expression as:

$$\eta_s = A^{VP} \bar{\eta} \tag{18}$$

It is noted that A^{VP} is a $6N_\beta N_\gamma \times 6$ matrix, containing the geometry parameters of the RUC and the material properties of the associated sub-cells. The A^{VP} matrix can be further partitioned into the $N_\beta N_\gamma$ entries, and each entry represents a 6×6 square matrix as

$$A^{VP} = \begin{bmatrix} A^{VP(11)} \\ A^{VP(12)} \\ \vdots \\ A^{VP(N_\beta N_\gamma)} \end{bmatrix} \tag{19}$$

Therefore, the components of the strain increment in the sub-cells can be expressed explicitly in terms of the overall strain increments as

$$\bar{\eta}^{(\beta\gamma)} = A^{VP(\beta\gamma)} \bar{\eta} \tag{20}$$

where $\beta = 1, \ldots, N_\beta$ and $\gamma = 1, \ldots, N_\gamma$.

The constitutive equations of each sub-cell $(\beta\gamma)$ is written as

$$\bar{\tau}_{ij}^{(\beta\gamma)} = C_{ijkl}^{VP(\beta\gamma)} \bar{\eta}_{kl}^{(\beta\gamma)} \tag{21}$$

where $C_{ijkl}^{VP(\beta\gamma)}$ denotes the elastic–plastic stiffness matrix of the sub-cell (β, γ). It is noted that when the sub-cells are represented as matrix material, the corresponding stiffness matrix $C^{VP(\beta\gamma)}$ is the same as $[C^M]$ provided in Eq. (14). Whereas the sub-cells are denoted as fiber, $C^{VP(\beta\gamma)}$ is equal to elastic stiffness matrix of the fiber. By substituting Eq. (20) into the sub-cell constitutive relation given in Eq. (21), the sub-cell stress increments are deduced as

$$\bar{\tau}^{(\beta\gamma)} = C^{VP(\beta\gamma)} A^{VP(\beta\gamma)} \bar{\eta} \tag{22}$$

Based on the average sense, the overall stress rate of the RUC is written as

$$\bar{\tau} = \frac{1}{hl} \sum_{\beta=1}^{N_\beta} \sum_{\gamma=1}^{N_\gamma} h_\beta l_\gamma \bar{\tau}^{(\beta\gamma)} \tag{23}$$

With Eqs. (22) and (23), the overall stress rate and strain rate relation of the RUC are established as

$$\bar{\tau} = B^{*VP} \bar{\eta} \tag{24}$$

where

$$B^{*VP} = \frac{1}{hl} \sum_{\beta=1}^{N_\beta} \sum_{\gamma=1}^{N_\gamma} h_\beta l_\gamma C^{VP(\beta\gamma)} A^{VP(\beta\gamma)} \tag{25}$$

With ingredient properties as well as RUC geometry, Eq. (25) can be used to model the responses of fiber composites. For the composites subjected to off-axis loading, the applied loading was decomposed into longitudinal, transverse and in-plane shear directions in the material principal directions. Subsequently, these stress components were employed as input in the overall stress and strain relation given in Eq. (24) for the calculation of the global strain. When the global strain was evaluated, it was substituted into Eq. (22) to calculate the local stress components of each sub-cell. The constitutive relation of each sub-cell was then updated by the calculated local stress components and through Eq. (25), the overall stress strain relation was obtained accordingly. By performing the numerical iteration together with the applied off-axis loading, the stress–strain curves of the composites with different fiber orientations were established.

2.4. Calculation of thermal residual stress

In order to investigate the thermal stress effect on the responses of fiber composites, the thermal residual stress induced during curing needs to be evaluated. These stress components can be calculated from the thermal–elastic analysis with the assistance of the GMC micromechanical model. For the sub-cell (β, γ), the constitutive equation can be described as

$$\bar{\tau}_{ij}^{(\beta\gamma)} = C_{ijkl}^{(\beta\gamma)} (\bar{\eta}_{kl}^{(\beta\gamma)} - \alpha^{(\beta\gamma)} \Delta T) \tag{26}$$

where the $C_{ijkl}^{(\beta\gamma)}$ represents the elastic stiffness matrix of the constituents; $\alpha^{(\beta\gamma)}$ is the thermal coefficient corresponding to the sub-cell (β, γ); and ΔT is the temperature change in

the RUC. The fiber composites were assumed to be stress free at curing temperature and the residual stresses were induced during the cooling process. Thus, ΔT indicates the temperature drop from the curing to the room temperature. It should be noted that the $C_{ijkl}^{(\beta\gamma)}$ presented in Eq. (26) is different from the $C_{ijkl}^{\mathrm{VP}(\beta\gamma)}$ given in Eq. (21) where both elastic and plastic deformations were considered. Based on the interface traction continuity between adjacent sub-cells, the relations for the sub-cell strain increment were deduced as

$$A_{\mathrm{M}}(\eta_{\mathrm{s}} - \alpha\Delta T) = 0 \tag{27}$$

It is noted that the expression of Eq. (27) is quite similar to that in Eq. (17), except that the matrix A_{M} is replaced by $A_{\mathrm{M}}^{\mathrm{VP}}$. This occurs because only elastic constitutive relation was utilized for deriving the thermal stress. In Eq. (27), $\alpha = \{\alpha^{(11)}, \alpha^{(12)}, \ldots, \alpha^{(N_\beta N_\gamma)}\}$ is denoted as the collection of coefficients of thermal expansion of all sub-cells. In conjunction with the displacement rate continuity given in Eq. (16), the traction continuity equations were further expressed as

$$\begin{bmatrix} A_{\mathrm{M}} \\ A_{\mathrm{G}} \end{bmatrix} \eta_{\mathrm{s}} - \begin{bmatrix} A_{\mathrm{M}} \\ 0 \end{bmatrix} \alpha\Delta T = \begin{bmatrix} 0 \\ J \end{bmatrix} \bar{\eta} \tag{28}$$

From Eq. (28), the sub-cell strain increments were correlated to the overall strain increments of the composites in terms of the temperature changes. Eq. (28) can be written in a simple form as

$$\eta_{\mathrm{s}} = \widetilde{A}^{-1} K \bar{\eta} + \widetilde{A}^{-1} \widetilde{A}^{p} \alpha\Delta T \tag{29}$$

where $\widetilde{A} = \begin{bmatrix} A_{\mathrm{M}} \\ A_{\mathrm{G}} \end{bmatrix}$, $\widetilde{A}^{\mathrm{p}} = \begin{bmatrix} A_{\mathrm{M}} \\ 0 \end{bmatrix}$ and $K = \begin{bmatrix} 0 \\ J \end{bmatrix}$. It is noted that both $\widetilde{A}$ and $\widetilde{A}^{\mathrm{p}}$ are square matrix with the dimensions $6N_\beta N_\gamma \times 6N_\beta N_\gamma$. The dimension of matrix K is $6N_\beta N_\gamma \times 6$. If $A = \widetilde{A}^{-1} K$ and $A^{\mathrm{p}} = \widetilde{A}^{-1}\widetilde{A}^{\mathrm{p}}$ are further defined, Eq. (29) can be simplified as

$$\eta_{\mathrm{s}} = A\bar{\eta} + A^{\mathrm{P}} \alpha\Delta T \tag{30}$$

The explicit form of Eq. (30) for each sub-cell (β, γ) was expressed as

$$\bar{\eta}^{(\beta\gamma)} = A^{(\beta\gamma)}\bar{\eta} + A^{\mathrm{P}(\beta\gamma)}\alpha^{(\beta\gamma)}\Delta T \tag{31}$$

By substituting Eq. (31) into Eq. (26), the thermal stress components for each sub-cell, after cooling, was written in terms of overall strain increment and temperature change as

$$\bar{\tau}^{(\beta\gamma)} = C^{(\beta\gamma)}(A^{(\beta\gamma)}\bar{\eta} + A^{\mathrm{P}(\beta\gamma)}\alpha^{(\beta\gamma)}\Delta T - \alpha^{(\beta\gamma)}\Delta T) \tag{32}$$

where $\bar{\eta}$ was the overall strain increment. Thus, once the overall deformation was determined, the residual stress for each sub-cell can be evaluated from Eq. (32). In addition, the overall stress states of the composites can be calculated based on the average concept of the stresses in each sub-cell. By substituting Eq. (32) into Eq. (23), the overall stress and strain relation of the composites corresponding to the temperature change was expressed as

Table 1
Material and thermal properties of the ingredients used in the GMC analysis

	Fiber	Matrix
E_1 (GPA)	234	3.4
E_2 (GPA)	14	
G_{12} (GPA)	27.6	
G_{23} (GPA)	5.5	
v_{12}	0.2	0.37
v_{23}	0.25	
α (1/°C)		1.18×10^{-4}
A		6.42×10^{-11}
n		4.11

$$\bar{\tau} = \frac{1}{hl}\sum_{\beta=1}^{\mathrm{N}_\beta}\sum_{\gamma=1}^{\mathrm{N}_\gamma} h_\beta l_\gamma C^{(\beta\gamma)}(A^{(\beta\gamma)}\bar{\eta} + A^{\mathrm{P}(\beta\gamma)}\alpha^{(\beta\gamma)}\Delta T - \alpha^{(\beta\gamma)}\Delta T) \tag{33}$$

It is noted that during cooling, there is no mechanical loading applied; therefore, the overall stress state of the composites should be equal to zero. In other words, the overall stress $\bar{\tau}$ in Eq. (33) is zero. Through mathematical manipulation, the overall strain components for the composites during the temperature change was derived as

$$\bar{\eta} = -B^{*^{-1}}\frac{1}{hl}\sum_{\beta=1}^{\mathrm{N}_\beta}\sum_{\gamma=1}^{\mathrm{N}_\gamma} h_\beta l_\gamma C^{(\beta\gamma)}(A^{\mathrm{P}(\beta\gamma)}\alpha^{(\beta\gamma)}\Delta T - \alpha^{(\beta\gamma)}\Delta T) \tag{34}$$

where $B^* = \frac{1}{hl}\sum_{\beta=1}^{\mathrm{N}_\beta}\sum_{\gamma=1}^{\mathrm{N}_\gamma} h_\beta l_\gamma C^{(\beta\gamma)}A^{(\beta\gamma)}$.

By substituting the overall strain components given by Eq. (34) into Eq. (32), the thermal residual stress of each sub-cell was evaluated. The thermal residual stress components were regarded as the initial stress states of each sub-cell that were then used to modify the initial constitutive relation of matrix phase provided in Eq. (11). All the ingredient properties of the fiber composites used for the following simulations are summarized in Table 1.

3. Results and discussion

3.1. Convergence of GMC analysis

In the GMC analysis, the RUC is divided into the numbers of sub-cells to represent either fiber or matrix phases. The number of the sub-cells is dependent on the microstructure of the RUC, including fiber geometry and packing arrangement. In general, when a RUC consists of round fibers embedded in matrix, significant amounts of sub-cells are required in an attempt to precisely simulate the circular geometry of the fiber. Nevertheless, as more sub-cells are taken into account, more computation time is needed. In order to compromise the computation time with the accuracy of the simulation, the converging tests have to be carried out on RUCs with different fiber arrangements, i.e., square edge, diagonal edge, and hexagonal packing. Fig. 3 demonstrates the RUC with square edge packing, containing 28×28 and 39×39 sub-cells,

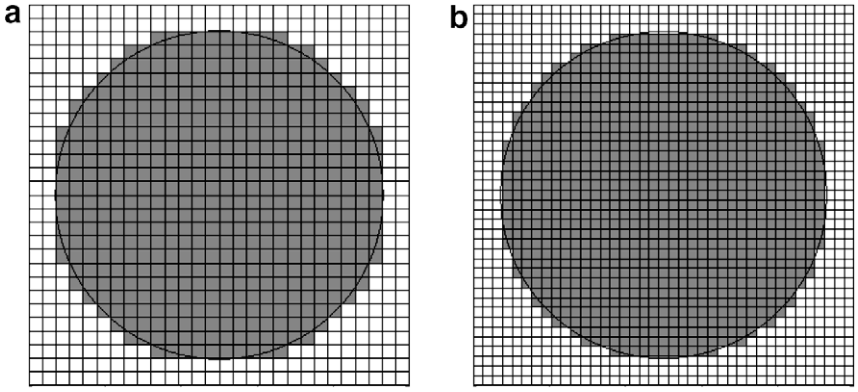

Fig. 3. a RUC with square edge packing portioned into 28×28 sub-cells (a) and 39×39 sub-cells (b), respectively.

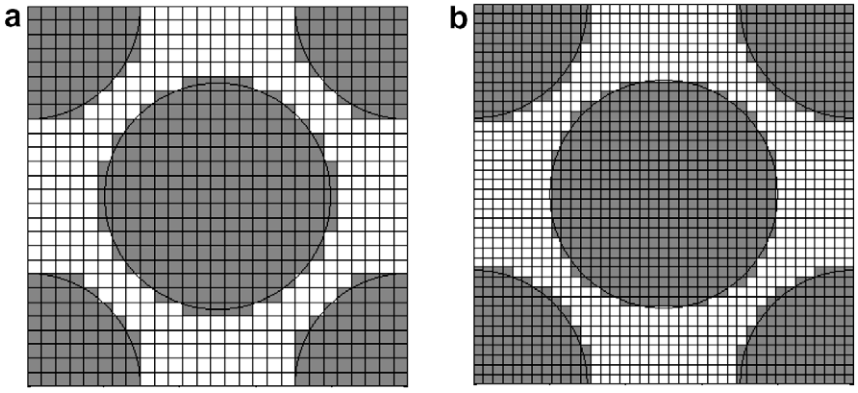

Fig. 4. a RUC with square diagonal packing partitioned into 27×27 sub-cells (a) and 39×39 sub-cells (b), respectively.

respectively, where the gray ones denote the fibers, and the white ones are the surrounding matrix. In addition, the RUCs with square diagonal packing and hexagonal packing were also partitioned into different sub-cells as shown in Figs. 4 and 5, respectively. Based on the different discretizations of RUCs, the stress and strain curves of the composites with 45°fiber orientation were calculated and the results were then compared in Fig. 6. It was shown that for each fiber arrangement, the constitutive curves obtained from the RUCs with coarse sub-cells demonstrate good agreements with those derived from the fine sub-cells. In light of the above verification, it was depicted that the rough partitions of the RUCs have accomplished the converged results and are suitable for characterizing the nonlinear responses of composites with round fibers

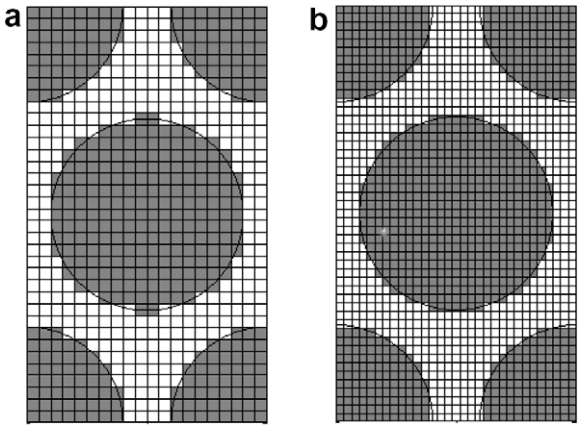

Fig. 5. a RUC with hexagonal packing partitioned into 20×35 sub-cells (a) and 31×49 sub-cells (b), respectively.

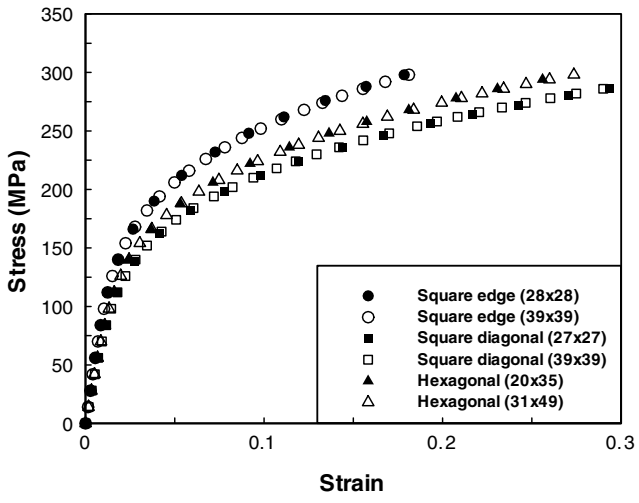

Fig. 6. Comparison of the stress and strain curves obtained from the RUCs with coarse sub-cells and refined sub-cells, respectively.

embedded. Moreover, the work by Pindera and Bednarcyk [5] also suggested that the RUC discretizations employed in the study are sufficient for accurate macro-level response and thus the results shown in Fig. 6 are not surprising.

3.2. Thermal stress effect

The nonlinear stress strain curves for 15°, 30°, 45°, 60° and 90° fiber composites with different fiber arrays are demonstrated, respectively, in Figs. 7–11. For comparison purposes, the composites disregarding the thermal stress effect were also enclosed in the Figures. In the simulations, the temperature drop was assumed to be 200°. Results show that the composites with different fiber arrays exhibit different stress and strain curves. Moreover, the square

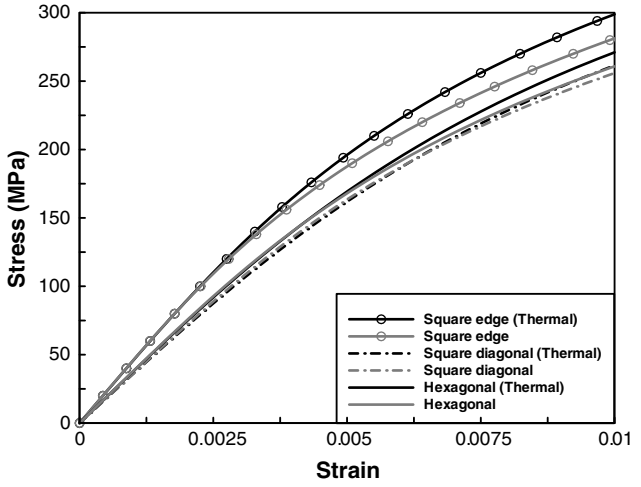

Fig. 7. Thermal residual stress effects on the stress and strain curves of 15° off-axis fiber composites with three different fiber arrays. (fiber volume fraction 60%).

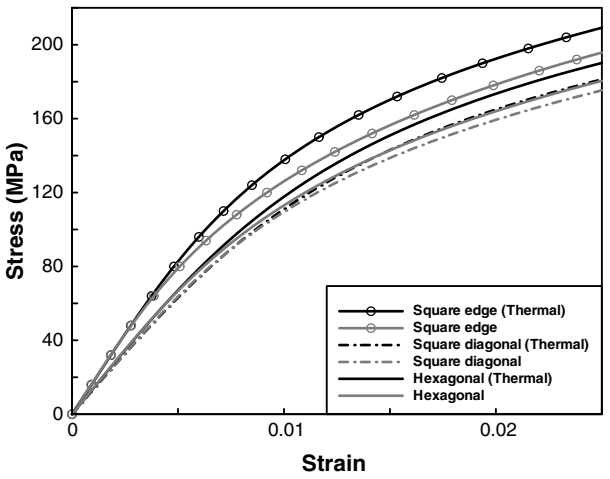

Fig. 8. Thermal residual stress effects on the stress and strain curves of 30° off-axis fiber composites with three different fiber arrays (fiber volume fraction 60%).

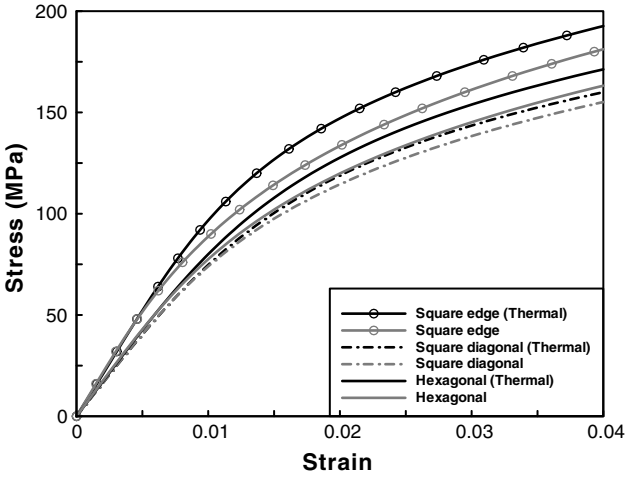

Fig. 9. Thermal residual stress effects on the stress and strain curves of 45° off-axis fiber composites with three different fiber arrays (fiber volume fraction 60%).

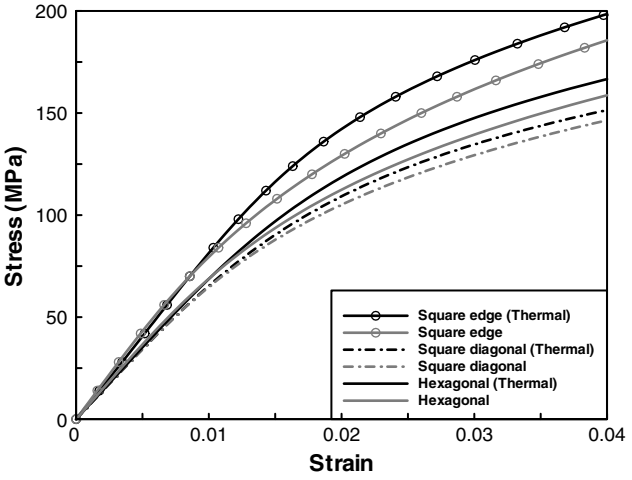

Fig. 10. Thermal residual stress effects on the stress and strain curves of 60° off-axis fiber composites with three different fiber arrays (fiber volume fraction 60%).

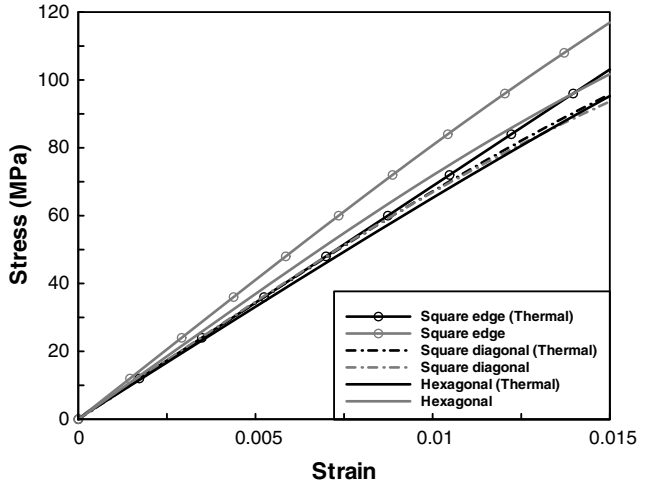

Fig. 11. Thermal residual stress effects on the stress and strain curves of 90° off-axis fiber composites with three different fiber arrays (fiber volume fraction 60%).

edge packing yields more stiffening behaviors than other fiber packing arrangements. Regarding the thermal stress effect, it is revealed that for the composites with square edge packing, the mechanical behaviors are affected appreciably by the thermal residual stress. Nevertheless, the composites with hexagonal packing and square diagonal packing are relatively less sensitive to the thermal residual stress. In addition, it was found that the effect of the fiber array architecture would be more important at high rather than low off-axis angles. Similarly, the residual stress appeared to have a greater effect at high rather than low off-axis angles for the square edge packing than the remaining packing. It is interesting to mention that for the 15°, 30°, 45°, 60° composites, the effect of residual stress seems to have the samples stiffer. In contrast, for the 90° composite, the constitutive behaviors become softer when the thermal residual stress is taken into account in the predictions.

4. Conclusions

The GMC micromechanical model was successfully extended to calculate the thermal residual stress of the fiber composites with different fiber arrays, i.e., square edge packing, square diagonal packing, and hexagonal packing. From the micromechanical analysis, it was indicated that for the composites with square edge packing, the constitutive behaviors are affected appreciably by the thermal residual stress. However, for the composites with hexagonal packing and square diagonal packing, the thermal residual stress exhibits little effects on their properties.

Acknowledgement

This research was supported by the National Science Council, Taiwan, under the Contract No. NSC 94-2212-E-009-017 to National Chiao Tung University.

References

[1] Paley M, Aboudi J. Micromechanical analysis of composites by the generalized cells model. Mech Mater 1992;14(2):127–39.
[2] Zhu C, Sun CT. Micromechanical modeling of fiber composites under off-axis loading. J Thermoplast Compos 2003;16(4):333–44.
[3] Hsu SY, Vogler TJ, Kyriakides S. Inelastic behavior of an AS4/PEEK composite under combined transverse compression and shear Park II: modeling. Int J Plasticity 1999;15(8):807–36.
[4] Orozco CE, Pindera MJ. Plastic analysis of complex microstructure composites using the generalized method of cells. AIAA J 1999;37(4):482–8.
[5] Pindera MJ, Bednarcyk BA. An efficient implementation of the generalized method of cells for unidirectional, multi-phased composites with complex microstructures. Compos Part B 1999;30(1):87–105.
[6] Pindera M-J, Herakovich CT, Becker W, Aboudi J. Nonlinear response of unidirectional boron/aluminum. J Compos Mater 1990;24(1):2–21.
[7] Zhou FH, Hashimoto R, Ogawa A, Sofue Y. Residual stress and its effect on yielding in SiC/Ti plate. JSME Int J Series A – Solid Mech Mater Eng 2006;49(1):25–31.
[8] Aghdam MM, Pavier MJ, Smith DJ. Micromechanics of off-axis loading of metal matrix composites using finite element analysis. Int J Solids Struct 2001;38(22–23):3905–25.
[9] Arnold SM, Pindera MJ, Wilt TE. Influence fiber architecture on the inelastic response of metal matrix composites. Int J Plasticity 1996;12(4):507–45.
[10] Drago AS, Pindera MJ. Micro-macromechanical analysis of heterogeneous materials: macroscopically homogeneous vs periodic microstructures. Compos Sci Technol 2007;67(6):1243–63.